

# Non-universal scalar-tensor theories and big bang nucleosynthesis

Alain Coc\*

*Centre de Spectrométrie Nucléaire et de Spectrométrie de Masse,  
IN2P3/CNRS/UPS, Bât. 104, 91405 Orsay Campus (France)*

Keith A. Olive†

*William I. Fine Theoretical Physics Institute,  
University of Minnesota, Minneapolis, MN 55455 (USA)*

Jean-Philippe Uzan‡ and Elisabeth Vangioni§

*Institut d'Astrophysique de Paris, UMR-7095 du CNRS,  
Université Pierre et Marie Curie, 98 bis bd Arago, 75014 Paris (France)*

(Dated: 6 aout 2008)

## Abstract

We investigate the constraints that can be set from big-bang nucleosynthesis on two classes of models: extended quintessence and scalar-tensor theories of gravity in which the equivalence principle between standard matter and dark matter is violated. In the latter case, and for a massless dilaton with quadratic couplings, the phase space of theories is investigated. We delineate those theories where attraction toward general relativity occurs. It is shown that big-bang nucleosynthesis sets more stringent constraints than those obtained from Solar system tests.

PACS numbers:

---

\*Electronic address: coc@csnsm.in2p3.fr

†Electronic address: olive@physics.unm.edu

‡Electronic address: uzan@iap.fr

§Electronic address: vangioni@iap.fr

## I. INTRODUCTION

While the late-time acceleration of the expansion of our universe seems to be a robust conclusion reached by several independent cosmological observations [1, 2, 3, 4, 5], its origin remains an open question [6, 7]. Various explanations for late-time acceleration have been proposed ranging from modifications of the laws of physics to questioning the Copernican principle [8, 9, 10]. If this principle holds we are led to the conclusion that our cosmological model requires the introduction of new physical degrees of freedom, often referred to as the “dark sector”. In this case, it is necessary to specify the interactions of these new fields, both their self interactions as well as their interactions with matter. There are several candidates for this new matter, the simplest being quintessence models [11], or a modification of general relativity (see Ref. [7] for a discussion on this distinction). Let us emphasize that the simplest model of all requires only the introduction of a single constant, the cosmological constant, and is at the moment in agreement with all available data [5, 12].

Among all the theories of gravitation beyond general relativity, scalar-tensor theories [13, 14] are a well motivated extension and may also be related to quintessence since they include one or more scalar fields universally coupled to matter. These theories are described by two functions, a potential describing the scalar self interactions, and a coupling function describing interaction of the scalar field to matter. Indeed, these theories depart from general relativity and are subject to many experimental constraints, particularly from the Solar system [15]. These deviations can however be larger on cosmological scales because, as long as the coupling function has a minimum, such theories can be dynamically attracted [16] toward general relativity during the evolution of the universe. More generally, when considering theories with a quintessence-like potential, it was shown [17, 18] that the theory can be attracted toward general relativity while the scalar field is driven toward the quintessence tracking solution, hence leading to models of extended quintessence that were advocated to be very generic for quintessence models [19, 20]. In that context, the deviations from general relativity can be constrained from big bang nucleosynthesis (BBN) [21, 22], the cosmic microwave background (CMB) [23], weak lensing [24] and the production of gravitational waves [25]. Interestingly, they can also lead [26] to an equation of state with  $p/\rho < -1$  for the dark energy.

It is indeed also possible that the new scalar field(s) do not couple universally to matter, as considered in Refs. [19, 20]. In this case, one expects a violation of the equivalence principle and a variation of the fundamental constants which can be used to constrain the equation of state of the dark energy [27]. However, such couplings are in general severely constrained [28, 29], with the exception of some particular cases such as the coupling to neutrinos [30] or dark matter.

When the scalar fields couple differently to the dark sector, there is almost no constraint from the equivalence principle on the interactions between dark matter (DM) and standard (or visible) matter (see however Ref. [31] for a possible test of the universality of free fall between DM and normal matter). Such a possibility was initially investigated in Ref. [32] in the particular case of Brans-Dicke theories and was recently revisited in Refs. [33]. These models can, in principle explain, the coincidence problem as well [34, 35, 36] and have been argued to naturally appear when the quintessence model is embedded in a supersymmetric construction [37].

In this article, we focus on big bang nucleosynthesis and build on our previous analysis [22, 38] that focused on the constraints that can be imposed on scalar-tensor theories of

gravity with a massless dilaton. We extend the results of Ref. [22] in two directions: (1) by considering extended quintessence models, i.e. a general scalar-tensor theory with a potential, and (2) by extending our formalism to models with a non-universal coupling between the dark matter sector and the visible sector. The theories considered in this article are first detailed in § II and both cases are studied respectively in § III and § IV. Most technicalities, such as the BBN data and Solar system constraints, are gathered in appendices.

## II. SCALAR-TENSOR THEORIES OF GRAVITY

### A. Definition of the model

In this article, we consider models in which gravity is described by a scalar-tensor theory and in which the strength of the scalar coupling may differ between CDM and ordinary matter. It follows that in the Einstein frame the action takes the form

$$S = \int \frac{d^4x}{16\pi G_*} \sqrt{-g_*} [R_* - 2g_*^{\mu\nu} \partial_\mu \varphi_* \partial_\nu \varphi_* - 4V(\varphi_*)] + S_V[A_V^2(\varphi_*)g_{\mu\nu}^*; \psi_V] + S_D[A_D^2(\varphi_*)g_{\mu\nu}^*; \psi_D]. \quad (2.1)$$

The action contains three arbitrary functions: the potential  $V$ , the couplings to ordinary matter,  $A_V$  ( $V$  for visible sector), and the coupling to CDM,  $A_D$  ( $D$  for dark sector). We will also consider cases where both coupling functions are set equal to each other.  $G_*$  is the bare gravitational constant from which we define  $\kappa_* = 8\pi G_*$ .

The Jordan frame is typically defined as the frame for which the metric is minimally coupled to matter. When  $A_V = A_D$ , there is a unique definition of the Jordan frame. With two coupling functions, we can define two different Jordan frames. Since standard clocks and rods are made of standard matter, we define the matter Jordan frame (MJF) to be that frame in which the standard matter fields are minimally coupled to the metric. The MJF metric will thus define length and time as measured by laboratory apparatus so that all observations (time, redshift, ...) have their standard interpretation in this frame. This is also the frame in which the nuclear reaction rates take their standard form, since they do not involve CDM. In this frame the stress-energy tensor of visible matter is conserved. The action then takes the form

$$S = \int \frac{d^4x}{16\pi G_*} \sqrt{-g} [F(\varphi)R - g^{\mu\nu} Z(\varphi) \varphi_{,\mu} \varphi_{,\nu} - 2U(\varphi)] + S_V[g_{\mu\nu}; \psi_V] + S_D[B^2(\varphi)g_{\mu\nu}; \psi_D] \quad (2.2)$$

after performing the conformal transformation

$$g_{\mu\nu}^* = F(\varphi)g_{\mu\nu} \quad (2.3)$$

with

$$\left(\frac{d\varphi_*}{d\varphi}\right)^2 = \frac{3}{4} \left[\frac{d \ln F(\varphi)}{d\varphi}\right]^2 + \frac{Z(\varphi)}{2F(\varphi)} \quad (2.4)$$

$$A_V(\varphi_*) = F^{-1/2}(\varphi) \quad (2.5)$$

$$2V(\varphi_*) = U(\varphi)F^{-2}(\varphi) \quad (2.6)$$

$$B(\varphi_*) = A_D/A_V. \quad (2.7)$$

We will denote all Einstein-frame quantities with a star (\*). The Einstein frame has the advantage of diagonalized the kinetic terms for the spin-0 and spin-2 degrees of freedom so that the degrees of freedom of the theory are more easily discussed. The strength of the couplings of the scalar field to the matter and CDM fields is characterized by

$$\alpha_i(\varphi_*) \equiv \frac{d \ln A_i}{d\varphi_*} \quad (2.8)$$

and we also define

$$\beta_i(\varphi_*) \equiv \frac{d\alpha_i}{d\varphi_*} \quad (2.9)$$

with  $i = V, D$ .

## B. Cosmological background equations

### 1. Space-time metrics

We consider a Friedmann-Lemaître universe with metric in the MJF

$$ds^2 = -dt^2 + R^2(t)\gamma_{ij}dx^i dx^j \quad (2.10)$$

where  $\gamma_{ij}$  is the spatial metric and  $R$  the scale factor. In the Einstein frame, the metric takes the same form but with a scale factor  $R_*$  and a time coordinate,  $t_*$  which are related to their MJF counterparts by

$$R = A_V(\varphi_*)R_*, \quad dt = A_V(\varphi_*)dt_* \quad (2.11)$$

and the redshifts are related by

$$1 + z = \frac{A_{V0}}{A_V}(1 + z_*) \quad (2.12)$$

### 2. Equations of motion in the Einstein frame

The Friedmann equations in this frame take a form similar to those of general relativity with a minimally coupled scalar field and a fluid,

$$3 \left( H_*^2 + \frac{K}{R_*^2} \right) = 8\pi G_* \rho_* + \psi_*^2 + 2V(\varphi_*) \quad (2.13)$$

$$-\frac{3}{R_*^2} \frac{d^2 R_*}{dt_*^2} = 4\pi G_* (\rho_* + 3P_*) + 2\psi_*^2 - 2V(\varphi_*) \quad (2.14)$$

where we have introduced  $H_* = d \ln R_*/dt_*$  and

$$\psi_* = d\varphi_*/dt_*. \quad (2.15)$$

$K$  is a positive, null or negative constant specifying the curvature of the spatial sections.  $\rho_*$  and  $P_*$  are the energy density and pressure of the total fluid.

In this model, the total energy can be split between the dark sector ( $\rho_D$ ) and the visible sector ( $\rho_V$ ),

$$\rho = \rho_V + \rho_D.$$

We assume that the dark sector component is described by a constant equation of state  $w_D$ , which is set to  $w_D = 0$  for CDM. The visible sector can be further decomposed between a pressureless matter component  $P_{\text{mat}} = 0$  and radiation ( $P_{\text{rad}} = \frac{1}{3}\rho_{\text{rad}}$ ), so that

$$\rho_V = \rho_{\text{mat}} + \rho_{\text{rad}}.$$

We stress that  $\alpha_{\text{rad}} = \alpha_{\text{mat}} = \alpha_V$  by construction, in order to satisfy the universality of free fall. In the Einstein frame, the evolution of these energy densities are dictated by the matter conservation equation,

$$\frac{d\rho_{i*}}{dt_*} + 3H_*(\rho_{i*} + P_{i*}) = \alpha_i(\varphi_*)(\rho_{i*} - 3P_{i*})\psi_*. \quad (2.16)$$

The r.h.s. term proportional to  $\psi_*$  is due to the scalar interaction. In our case it reduces to 0,  $\alpha_V\rho_{\text{mat*}}\psi_*$  and  $\alpha_D\rho_{D*}\psi_*$  for the radiation, standard matter and CDM.

The evolution of the scalar field is a Klein-Gordon equation

$$\frac{d\psi_*}{dt_*} + 3H_*\psi_* = -\frac{dV}{d\varphi_*} - 4\pi G_* \sum_i \alpha_i(\varphi_*)(\rho_{i*} - 3P_{i*}), \quad (2.17)$$

where the sum is taken over  $i = \text{rad}, \text{mat}, D$ . The coupling term reduces to

$$-4\pi G_* \sum_i \alpha_i(\varphi_*)(\rho_{i*} - 3P_{i*}) = -4\pi G_* [\alpha_D\rho_{D*} + \alpha_V\rho_{\text{mat*}}].$$

### 3. Implementing BBN

The nuclear reaction network takes its standard form in the matter Jordan frame, where the Lagrangian for the visible sector is not affected by the existence of the scalar field so that the cross-sections etc. . . also take their standard form.

To compute the light elements abundances during BBN, one only needs to know the expansion rate history,  $H(z)$ , from deep in the radiation era up to today. It is thus convenient to express the Hubble parameter in the MJF in terms of the one in the Einstein frame, using Eq. (2.11), as

$$A_V H = [H_* + \alpha_V(\varphi_*)\psi_*]. \quad (2.18)$$

Eq. (2.18) can also be expressed in the simple form

$$A_V H = H_* \left[ 1 + \alpha_V(\varphi_*) \frac{d\varphi_*}{dp} \right] \quad (2.19)$$

where  $p$  is the number of e-folds of expansion in Einstein frame,

$$p = -\ln(1 + z_*). \quad (2.20)$$

Our numerical strategy follows exactly the one developed in Ref. [22]. We solve the Einstein equation in the Einstein frame (see appendix A) and then deduce  $H(z)$  from Eq. (2.18) to compute the production of the light elements.

#### 4. Evolution the energy densities

The system of equations (A1-A7) are expressed in terms of the energy densities of the various components. Interestingly, these can be derived analytically. In the MJF, the densities are related to their Einstein frame counterpart by

$$\rho_* = A_V^4 \rho, \quad P_* = A_V^4 P. \quad (2.21)$$

For matter in the visible sector, Eq. (2.16) takes the simple form

$$\dot{\rho}_V + 3H(\rho_V + P_V) = 0 \quad (2.22)$$

and is trivially integrated to get

$$\rho_{Vi} = \rho_{Vi0}(1+z)^{3(1+w_i)}, \quad (2.23)$$

for any component of the visible sector (i.e.  $i = \text{rad, mat}$ ) with a constant equation of state and where  $z$  is the redshift defined by  $1+z = R_0/R$ . Using Eqs. (2.11-2.12), we obtain the evolution of the energy density in the Einstein frame

$$\rho_{Vi*} = \rho_{Vi0*} \left( \frac{A_V}{A_{V0}} \right)^{4-3(1+w_i)} (1+z_*)^{3(1+w_i)}, \quad (2.24)$$

where  $\rho_{i0*} = A_{V0}^4 \rho_{Vi0}$ . We can also define the associated density parameter by

$$\Omega_{Vi0} \equiv \frac{8\pi G_* A_{V0}^2}{3H_0^2} \rho_{Vi0}. \quad (2.25)$$

In the dark sector, the conservation equation has a source term in the MJF,

$$\dot{\rho}_D + 3H(\rho_D + P_D) = A_V^{-1}(\alpha_D - \alpha_V)(\rho_D - 3P_D)\psi_*. \quad (2.26)$$

This equation can be obtained by plugging Eq. (2.21) into Eq. (2.16) for  $i = D$  and using the relation (2.11) to shift to derivative with respect to  $t_*$ . Interestingly, we can find the solution of this equation analytically. In the CDM Jordan frame, defined by  $\tilde{t}$  and scale factor  $\tilde{R}$ , CDM is not coupled to the scalar field so that  $\tilde{\rho}_D \propto \tilde{R}^{-3(1+w_D)}$ . Going back to the Einstein frame, this implies that

$$\rho_{D*} \propto R_*^{-3(1+w_D)} A_D^{4-3(1+w_D)}$$

and then in MJF,

$$\rho_D = \rho_{D0} \left( \frac{A_D/A_V}{A_{D0}/A_{V0}} \right)^{4-3(1+w_D)} (1+z)^{3(1+w_D)}. \quad (2.27)$$

Indeed, if the coupling of the scalar field is universal, the dark matter and normal matter satisfy the same evolution equation. In a general model where  $A_V \neq A_D$ , the two matter components evolve differently. This is related to the fact that both forms of matter do not experience the same coupling to the scalar field.

We deduce that the ratio between the dark matter and baryonic matter components is a priori not constant during the evolution of the universe. It is given by

$$\frac{\rho_{D*}}{\rho_{m*}} = \frac{\rho_D}{\rho_m} = \frac{\rho_{D0}}{\rho_{m0}} \frac{A_{V0}}{A_{D0}} \frac{A_D}{A_V}(\varphi_*) \equiv \Xi_0 \frac{B(\varphi_*)}{B_0}, \quad (2.28)$$

with  $\Xi_0 \equiv \rho_{D0}/\rho_{m0}$  and we define  $\tilde{\Xi}_0 \equiv \Xi_0/B_0$ . This is a main feature of this class of models, which distinguishes it from universal scalar-tensor theories.

Finally, the energy density of the scalar field in the Einstein frame is given from Eq. (2.13) by

$$\rho_{\varphi*} = \frac{1}{8\pi G_*} \left[ \left( \frac{d\varphi_*}{dt_*} \right)^2 + 2V(\varphi_*) \right] \quad (2.29)$$

so that its energy density in the matter Jordan frame is

$$\rho_\varphi = A_V^{-4} \rho_{\varphi*}. \quad (2.30)$$

### III. AN EXTENDED QUINTESSENCE MODEL

Before we move on to the most general type of models with two coupling functions, we consider first an extension of the models considered in Ref. [22] with self-interaction potentials, but with  $A_V = A_D$ . Our first examples are thus models of extended quintessence in which the scalar field accounts for the late time acceleration of the Universe while also being responsible for a scalar interaction. Given the framework we have set up in the previous section, we can now examine the consequences on BBN of several choices of quintessence models.

As a first example, we consider an extended quintessence model of the runaway type with a potential and coupling function given by

$$V = M^2 \varphi_*^{-a}, \quad \ln A = C \varphi_*^{-b}, \quad (3.1)$$

where  $a$ ,  $b$  and  $C$  are all positive and the mass scale  $M \ll \kappa^{-1/2}$  must be tuned so that  $\Omega_\varphi \sim \Omega_\Lambda$  today. It follows that

$$\alpha = -Cb\varphi_*^{-b-1}. \quad (3.2)$$

When  $C = 0$ , this model is a standard quintessence model with an inverse power law potential. The dynamics of this model has been investigated in depth. In particular, there exist scaling solutions with attractors of the dynamics of the scalar field which behaves as a perfect fluid with an effective equation of state

$$w_\varphi = \frac{wa - 2}{a + 2}, \quad (3.3)$$

where  $w$  is the equation of state of the fluid that dominates the matter content of the universe. Figure 1 depicts the evolution of the energy densities as a function of the redshift in this case and shows the quintessence attractor mechanism typical for inverse power law quintessence potentials when gravity is described by general relativity (i.e.  $C = 0$ ).

When  $C \neq 0$ , and as discussed in detail in Ref. [22], we expect two main effects. First during BBN, the field dynamics is modified during electron-positron annihilation and then the late time dynamics is modified because of the coupling to non-relativistic matter. Let us investigate them by assuming that  $V = 0$ .

As detailed in § III.A.2 of Ref. [22], the dynamics during electron-positron annihilation is governed by the equation

$$\frac{2}{3 - \varphi_*'^2} \varphi_*'' + \frac{2}{3} \varphi_*' = -\alpha(\varphi_*) \Sigma_e,$$

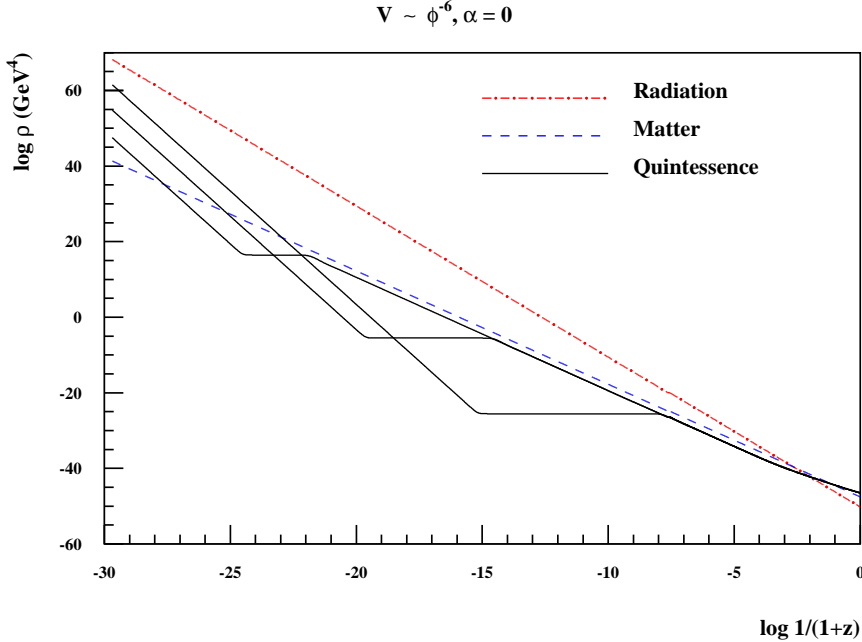


FIG. 1: Evolution of the energy densities of the matter, radiation and scalar field as a function of the redshift for a model with potential (3.1) with  $a = 6$ ,  $C = 0$  and  $M = 4 \times 10^{-17} \text{ s}^{-1}$  for different initial conditions,  $\phi_{\text{in}} = 2 \times 10^{-16}$ ,  $6 \times 10^{-16}$ , and  $2 \times 10^{-15}$ . The field initially enters a kinetic regime so that  $\rho_\phi \propto (1+z)^6$  and then reaches a slow-roll regime until its energy density is of the same order of magnitude as that of the matter and radiation. At this stage, it enters a tracking regime where its effective equation of state is  $w_\phi = 0$  and  $w_\phi = -1/4$  during the radiation and matter era respectively. It follows that the scalar field always ends up dominating the matter content of the universe at late times and gives rise to an accelerated phase of expansion.

where  $\Sigma_e \equiv (\rho_e - 3P_e)/\rho_{\text{rad}}$  and prime denotes a derivative with respect to  $p$ . In a non-kinetic regime, this equation can be approximated by

$$\varphi_*'' + \varphi_*' = \frac{3}{2}Cb\varphi_*^{-b-1}\Sigma_e.$$

As in the case of a quadratic coupling [22], the field is frozen to some initial value  $\varphi_{\text{in}*}$  during the radiation era [39] prior to the electron-positron annihilation. Then the source term  $\Sigma_e$  acts temporarily inducing the evolution of  $\varphi_*$  which then settles to another constant value  $\varphi_{\text{out}*}$  in the radiation era. Because  $\ln A$  does not have a minimum, the field will shift towards larger values so that  $\varphi_{\text{out}*} > \varphi_{\text{in}*}$ .

During the matter era, the evolution equation reduces to

$$\frac{2}{3 - \varphi_*^2}\varphi_*'' + \varphi_*' = -\alpha(\varphi_*) = Cb\varphi_*^{-b-1},$$

Since the minimum of the coupling function is at infinity, it follows that the scalar field is simply attracted toward this value and does not undergo damped oscillations as in the case of a quadratic coupling. In particular, in the slow-roll regime, it behaves as

$$\varphi_* = \varphi_{\text{eq}*} \left[ 1 + (2+b) \frac{Cb}{\varphi_{\text{eq}*}^{2+b}} (p - p_{\text{eq}}) \right]^{\frac{1}{2+b}},$$

where  $p_{\text{eq}}$  is the value of  $p$  at the matter-radiation equality.

In the general case where both the potential and the coupling are effective, the solution is first attracted toward the quintessence scaling solution during the radiation era during which the coupling is not efficient. The various mass thresholds further drive  $\varphi_*$  toward larger values so that it reaches the quintessence tracking solution more rapidly. Then, during the matter era, the evolution is driven by the potential and coupling which both drive  $\varphi_*$  to infinity so that the scalar-tensor theory is attracted toward general relativity. Figure 2 shows the magnitude of these effects.

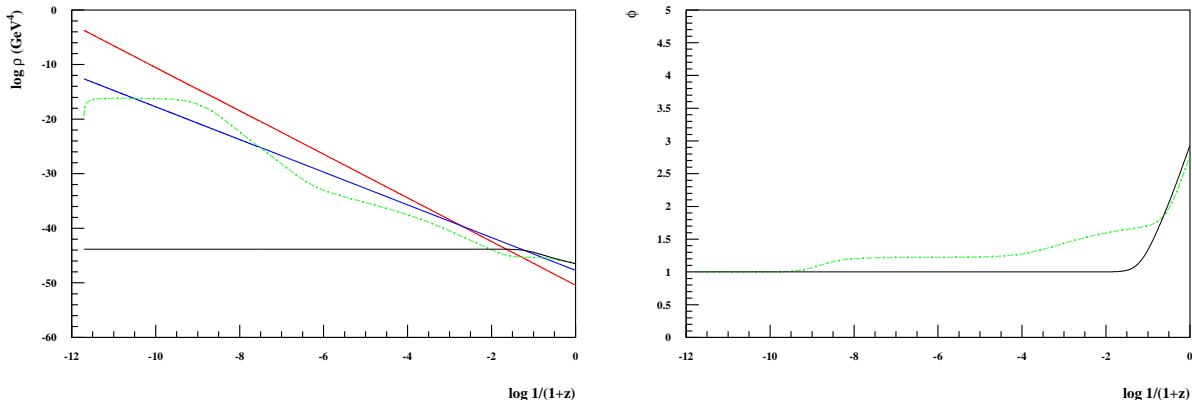


FIG. 2: (Left): Evolution of the energy densities of the matter (blue line), radiation (red line) and scalar field as a function of the redshift for a model with potential (3.1) with  $\phi(z = 10^{12}) = 1$ ,  $a = b = 6$  and  $C = 0$  (solid black line) or  $C = 0.2$  (dash dotted green line). (Right): Evolution of  $\phi$  for the same conditions.

Quintessence fields coupled to the Maxwell term,  $F^2$ , in the action, will induce a variation of the fine structure constant. There are a few models [40, 41] which can simultaneously account for the purported variation in quasar absorption systems [42] and the Oklo and meteoritic constraints [43, 44, 45]. Here we consider the model of Ref. [40] with the potential

$$V(\varphi_*) = V_0 \exp\left(\frac{\lambda}{2}\varphi_*^2\right), \quad (3.4)$$

which is representative of a class of models which possess a minimum in the self-interaction potential and is closely related to the one studied in Refs. [46, 47]. The potential is normalized by taking  $V_0$  to correspond to the present vacuum energy density. The coupling function in this model is also specified and related to the potential

$$A(\varphi_*) = \left[\frac{b + V(\varphi_*)/V_0}{1 + b}\right]^n \quad (3.5)$$

where  $1 + b > 0$ . Its main feature is to have a common minimum with that of the potential, and allows the system to recover general relativity when the scalar field is at the minimum. This is in the spirit of the least coupling principle [16] whose goal is to suppress the scalar interaction when the field has reached its minimum. Note that in Ref. [40] where the scalar field was also responsible for a variation of the fine structure constant, constraints were

derived such that  $n$  needed to be very small. In the current context, the field is universally coupled so that it is responsible only for a variation of the gravitational constant, which is much less constrained than the time variation of the fine structure constant [28, 29].

For small values of the field  $\varphi_*$ ,  $A$  can be approximated by  $1 + n\lambda\varphi_*^2/2(1+b)$ , so that we can write

$$\alpha \approx \frac{n\lambda\varphi_*}{1+b} \quad \beta \approx \frac{n\lambda}{1+b} \quad (3.6)$$

For  $\beta = 0$ , we show the evolution of  $\varphi_*$  as a function of redshift in Figure 3a. We see that for most of the evolution  $\varphi_*$  is constant largely due to the very small value of  $V_0$ . At late times, the field evolves toward the minimum at the origin. This type of model (with very small  $\beta$ ) was constructed to account for the possible evolution of the fine structure constant. In panel b), we show the corresponding evolution when  $\beta$  takes values 0.1, 1, and 10. We see that as  $\beta$  is increased, the evolution of  $\varphi_*$  begins at higher redshift. When  $\beta = 1(10)$ , we also see that the field undergoes a few (many) oscillations about the origin.

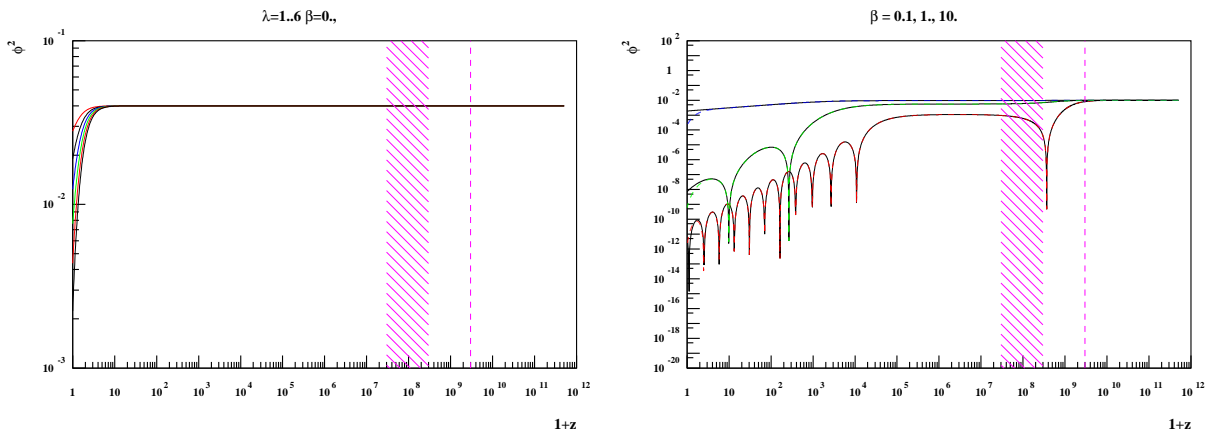


FIG. 3: Evolution of  $\varphi_*$  as a function of the redshift for models with potential and coupling defined in Eqs. (3.4-3.5). (Left): we set  $\beta=0$  and  $\lambda = 1, 2, 3, 4, 5$  and  $6$ , so that we are dealing with a quintessence model and no modification of general relativity. (Right): we set  $\beta= 0.1, 1,$  and  $10$ . without a potential (solid) or with a potential and  $\lambda = 6$  (dashed). Differences with and without a potential appear only at the very late times. The vertical dashed line corresponds to the time of  $n/p$  freeze-out and the shaded region to the epoch of BBN.

#### IV. NON-UNIVERSAL MASSLESS DILATON WITH QUADRATIC COUPLINGS

We now consider models in which  $A_V \neq A_D$ . For simplicity we focus on models with a constant potential and we assume that the two coupling functions are quadratic, which gives us a natural extension of the model studied in Ref. [22]. We set

$$A_V = \exp\left(\frac{1}{2}\beta_V\varphi_*^2\right), \quad A_D = \exp\left(\frac{1}{2}\beta_D\varphi_*^2\right), \quad V = V_0, \quad (4.1)$$

and we define

$$a_i(\varphi_*) = \ln[A_i(\varphi_*)]. \quad (4.2)$$

This is also a generalization of Ref. [32] which was restricted to Brans-Dicke models.

$V_0$  is constant so that the scalar degree of freedom remains massless. As in the previous model considered [Eq. (3.4)] it is associated with a constant energy density in the Einstein frame

$$\rho_{\Lambda^*} \equiv V_0/4\pi G_* , \quad (4.3)$$

but scales as  $A_V^{-4}$  in the matter Jordan frame. It follows that the total energy density is  $\rho_T = \rho + \rho_{\Lambda^*}$ . Note that the couplings are such that this component is not coupled to  $\varphi_*$ , that is

$$A_{\Lambda} = 1 , \quad \alpha_{\Lambda} = 0. \quad (4.4)$$

We note that the tests on the deviations from general relativity in the Solar system involve only  $\alpha_V$  and  $\beta_V$  since they are performed with ordinary matter.

## A. Dynamics

### 1. Reduced equation

The dynamics of this non-universal system can be discussed using  $p$  as a time variable. Since  $dp = H_* dt_*$ , we can deduce that  $\psi_* = H_* \varphi'_*$  and we can rewrite the Friedmann equation (A3) as

$$(3 - \varphi_*'^2)H_*^2 = 8\pi G_*(\rho_* + \rho_{\Lambda^*}). \quad (4.5)$$

The derivative of Eq. (A2) with respect to  $p$  implies that

$$\varphi_*'' + \left( \frac{H_*'}{H_*} + 3 \right) \varphi_*' = -\frac{4\pi G_*}{H_*^2} \sum_i \alpha_i (1 - 3w_i) \rho_{i*}.$$

Now, it can be checked that

$$\frac{H_*'}{H_*} = -\frac{1'}{2} (3 - \varphi_*'^2)(1 + \tilde{w})\varphi_*' - \varphi_*'^2,$$

where  $\tilde{w}$  includes the contribution of the cosmological constant,

$$\rho_*(1 + w) = (\rho_* + \rho_{\Lambda^*})(1 + \tilde{w}) . \quad (4.6)$$

Thus, we conclude that the dynamics is described by

$$\frac{2}{3 - \varphi_*'^2} \varphi_*'' + (1 - \tilde{w})\varphi_*' = - \sum_i \alpha_i (1 - 3w_i) \frac{\rho_{i*}}{\rho_* + \rho_{\Lambda^*}} \quad (4.7)$$

$$= -\alpha_V \frac{\rho_{\text{mat}*}}{\rho_* + \rho_{\Lambda^*}} - \alpha_D (1 - 3w_D) \frac{\rho_{D*}}{\rho_* + \rho_{\Lambda^*}} \quad (4.8)$$

This generalizes the equation used in Refs. [16, 21, 22] to the case of two couplings. We emphasize that this equation holds only when  $V = V_0$  is constant and for  $K = 0$ .

It is interesting to note that if the cosmological constant is negligible and if the dark matter and the baryonic matter have the same equation of state  $w_D = w$  then Eq. (4.7) is equivalent to the one that would be obtained with one single fluid with equation of state  $w$  with a universal scalar-tensor theory with an effective coupling function

$$A_{\text{eff}}(\varphi_*) = A_V(\varphi_*) + \tilde{\Xi}_0 A_D(\varphi_*), \quad (4.9)$$

which depends on the ratio of dark matter and baryonic matter, as well as initial conditions, through  $\tilde{\Xi}_0$ .

## 2. Phase space

Neglecting the cosmological constant, which dominates only in the last e-fold, Eq. (4.7) reduces to

$$\frac{2}{3 - \varphi_*'^2} \varphi_*'' + (1 - w) \varphi_*' = - \frac{\beta_V + \beta_D \Xi_0 e^{\frac{1}{2}(\beta_D - \beta_V)(\varphi_*^2 - \varphi_{*0}^2)}}{1 + \Xi_0 e^{\frac{1}{2}(\beta_D - \beta_V)(\varphi_*^2 - \varphi_{*0}^2)} + \frac{\rho_{\text{rad}}}{\rho_{\text{mat}}}} \varphi_*. \quad (4.10)$$

Let us focus on the matter dominated era. Eq. (4.10) indicates that the attraction toward general relativity will depend crucially on the relative signs of  $\beta_V$  and  $\beta_D$  and on the form of the effective coupling function  $A_{\text{eff}}$  which enters on the r.h.s. of the Klein-Gordon equation.

We have the following different possibilities:

- $\beta_V = 0$ : the scalar-tensor theory is pure general relativity in the visible sector. Only cosmology can set constraints on  $\beta_D$  while all Solar system constraints are always satisfied.
- $\beta_D = 0$ : the theory is attracted toward general relativity only if  $\beta_V > 0$ .
- $\beta_D > 0$  and  $\beta_V > 0$ :  $a_V$  and  $a_D$  have the same minimum at  $\varphi_* = 0$  so that the effective function  $a_{\text{eff}}$  also has a unique minimum in  $\varphi_* = 0$  which is an attractor of the dynamics. The scalar-tensor theory is thus attracted towards general relativity, both for the matter and the dark sectors, during electron-positron annihilation and the late time matter era when  $\varphi_* \rightarrow 0$ .
- $\beta_D < 0$  and  $\beta_V < 0$ : Neither  $a_V$  nor  $a_D$  have a minimum and thus  $a_{\text{eff}}$  does not have a minimum.  $\varphi_*$  runs to infinity when either matter or dark matter is dominant. The scalar-tensor theory thus drifts away from general relativity. We shall thus discard this case since local constraints can be satisfied only at the price of an extreme fine-tuning of the initial conditions.
- $\beta_D \beta_V < 0$ : This situation is more complex.  $\varphi_* = 0$  is always an extremum of  $a_{\text{eff}}$  but not necessary a minimum. Two conditions have to be considered.

First, if

$$\Phi \equiv \frac{2}{\beta_D - \beta_V} \ln \left( - \frac{\beta_V}{\beta_D \tilde{\Xi}_0} \right) < 0, \quad (4.11)$$

$a_{\text{eff}}$  has a *unique* extremum at  $\varphi_* = 0$  otherwise it has two others given by

$$\varphi_{\text{att}*}^2 = \varphi_{0*}^2 + \frac{2}{\beta_D - \beta_V} \ln \left( - \frac{\beta_V}{\beta_D} \frac{\rho_{\text{mat}0}}{\rho_{D0}} \right). \quad (4.12)$$

Second, if

$$\tilde{\beta} \equiv \beta_V + \tilde{\Xi}_0 \beta_D > 0, \quad (4.13)$$

the extremum at  $\varphi_* = 0$  is a minimum.

The signs of these two functions set the shape of the function  $a_{\text{eff}}$  which determines the late time attractor of the Klein-Gordon equation. Note that  $\Phi$  changes sign when  $\tilde{\beta}$  does. Fig. 4 summarizes the various possibilities in the phase space while Fig. 5 depicts the modification to  $a_{\text{eff}}$  when the values of  $\beta_D$  and  $\beta_V$  vary and when the signs of  $\Phi$  and  $\tilde{\beta}$  change.

Given the shape of  $a_{\text{eff}}$ , we have two possibilities for the late time dynamics:

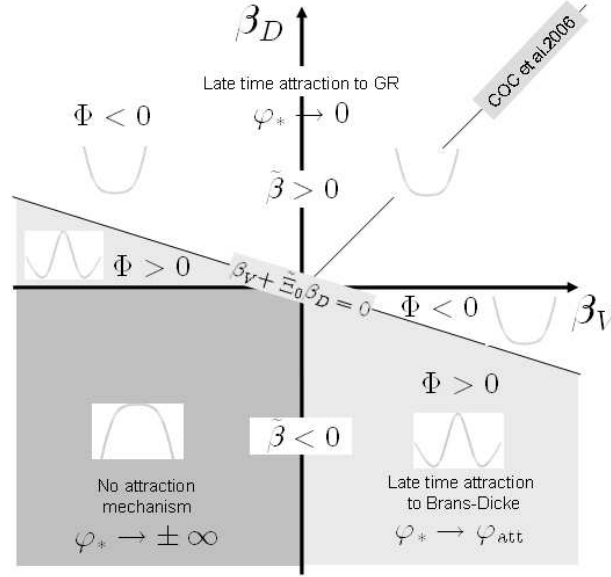


FIG. 4: The  $(\beta_V, \beta_D)$  parameter space with the signs of  $\Phi$  and  $\tilde{\beta}$  [defined in Eqs. (4.11) and (4.13)] which determine the shape of  $a_{\text{eff}}$  and thus the late time attractors of the Klein-Gordon equation. Three possibilities appear: late time attraction toward general relativity for  $\tilde{\beta} > 0$ , late time attraction toward a Brans-Dicke theory when  $\tilde{\beta} < 0$  and  $\beta_D \beta_V < 0$  and runaway when  $\beta_D < 0$  and  $\beta_V < 0$ . The field is respectively attracted toward 0,  $\pm\varphi_{\text{att}}$  and  $\pm\infty$ .

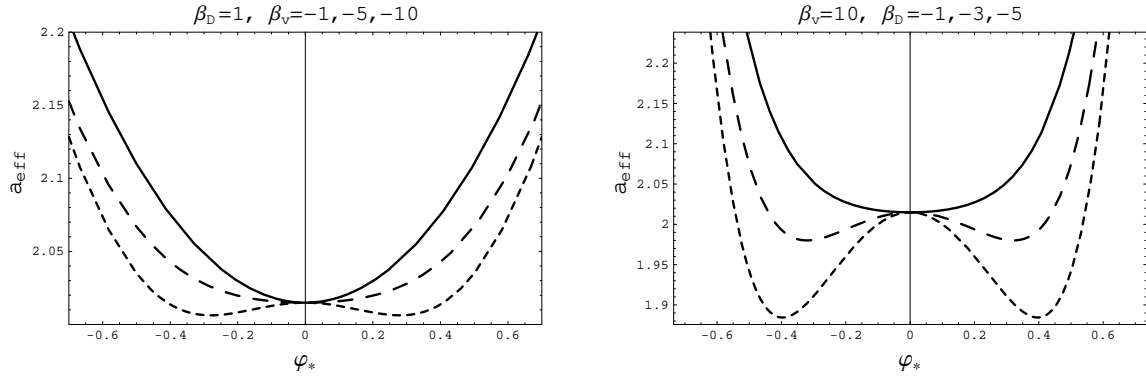


FIG. 5: Modification of the shape of  $a_{\text{eff}}$  with the values of  $\beta_D$  and  $\beta_V$  and with the signs of  $\Phi$  and  $\tilde{\beta}$ .

- $\varphi_* = 0$  is the only minimum. The Klein-Gordon equation involves  $A_{\text{eff}}$  so that  $\varphi_*$  is attracted toward 0 during the matter era. Since this corresponds to the minimum of  $a_V$  and  $a_D$ , the scalar-tensor is also attracted toward general relativity.
- $\varphi_* = 0$  is a local maximum. In this case  $\varphi_*$  is attracted toward  $\varphi_{\text{att}} \neq 0$ . This does not coincide with a minimum of  $a_V$  and  $\alpha_V \rightarrow \beta_V \varphi_{\text{att}}$ . The scalar-tensor is thus attracted towards a Brans-Dicke theory, that is a scalar tensor theory with  $\ln A = \lambda \varphi_*$ . Fig. 6 illustrates such a case where  $\varphi_*$  cannot relax to the minimum of the coupling function  $A_V$  because the dynamics is dictated by  $A_{\text{eff}}$ . It follows

from Eq. (4.11) that

$$\alpha_V^2 \rightarrow \alpha_{V0}^2 + 2 \frac{\beta_V}{\beta_D - \beta_V} \ln \left( -\frac{\beta_V}{\beta_D \Xi_0} \right).$$

According to the value of the parameters, the asymptotic Brans-Dicke parameter can be compatible with the observational constraints. Indeed, the theory can be temporarily attracted toward general relativity due to the mass thresholds in the primordial universe if  $\beta_V > 0$ . In this case,  $\alpha_{V0}$  can be low enough to pass Solar system tests.

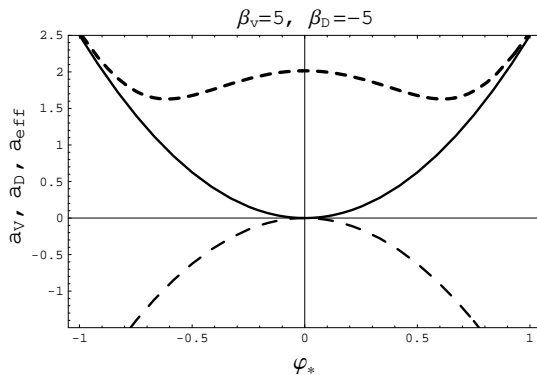


FIG. 6: When the minimum of  $a_{\text{eff}}$  (dashed line) differs from the one of  $a_V$  (solid line) and  $a_D$  (long dashed line), the dynamics of the scalar field drives  $\varphi_*$  to a minimum of  $A_{\text{eff}}$  so that the scalar-tensor theory is attracted toward a Brans-Dicke theory.

As discussed above, Figures 4 and 7 summarize the field dynamics. Three possibilities appear: late time attraction towards general relativity for  $\tilde{\beta} > 0$ , late time attraction toward a Brans-Dicke theory when  $\tilde{\beta} < 0$  and  $\beta_D \beta_V < 0$  and runaway when  $\beta_D < 0$  and  $\beta_V < 0$ . In each of these cases, the field is attracted towards  $0$ ,  $\pm\varphi_{\text{att}}$  and  $\pm\infty$ , respectively. Only models such that the effective parameter  $\tilde{\beta}$  is positive, enjoy a late time attraction toward general relativity.

Fig. 7 connects the phase space  $(\beta_V, \beta_D)$  with specific examples of model evolution which highlight the different possibilities. Fig. 4 has been miniaturized in the lower left of Fig. 7 and with evolutionary examples for each quadrant except that for which  $\beta_D, \beta_V < 0$  and the theory exhibits runaway behavior.

In the upper left of Fig. 7, we show the evolution of  $\varphi_*^2$  as a function of redshift for  $\tilde{\beta} = -1, 0, +1$ , all with  $\beta_V = -10$ . If  $\beta_V$  is negative the theory is dragged away from general relativity. This is seen by the increase in  $\varphi_*^2$  prior to BBN. This could be compensated at late times if  $\tilde{\beta} > 0$  as seen in the lower curve with  $\tilde{\beta} = 1$  which undergoes two oscillations about the minimum. Note that when  $\tilde{\beta} = 0$  the Klein-Gordon equation has no source term even after the end of the radiation era so that  $\varphi_*$  remains frozen to the same value than during the radiation era. The scalar-tensor theory can be attracted toward general relativity only due to the effects of the mass thresholds. Therefore no evolution is seen after BBN

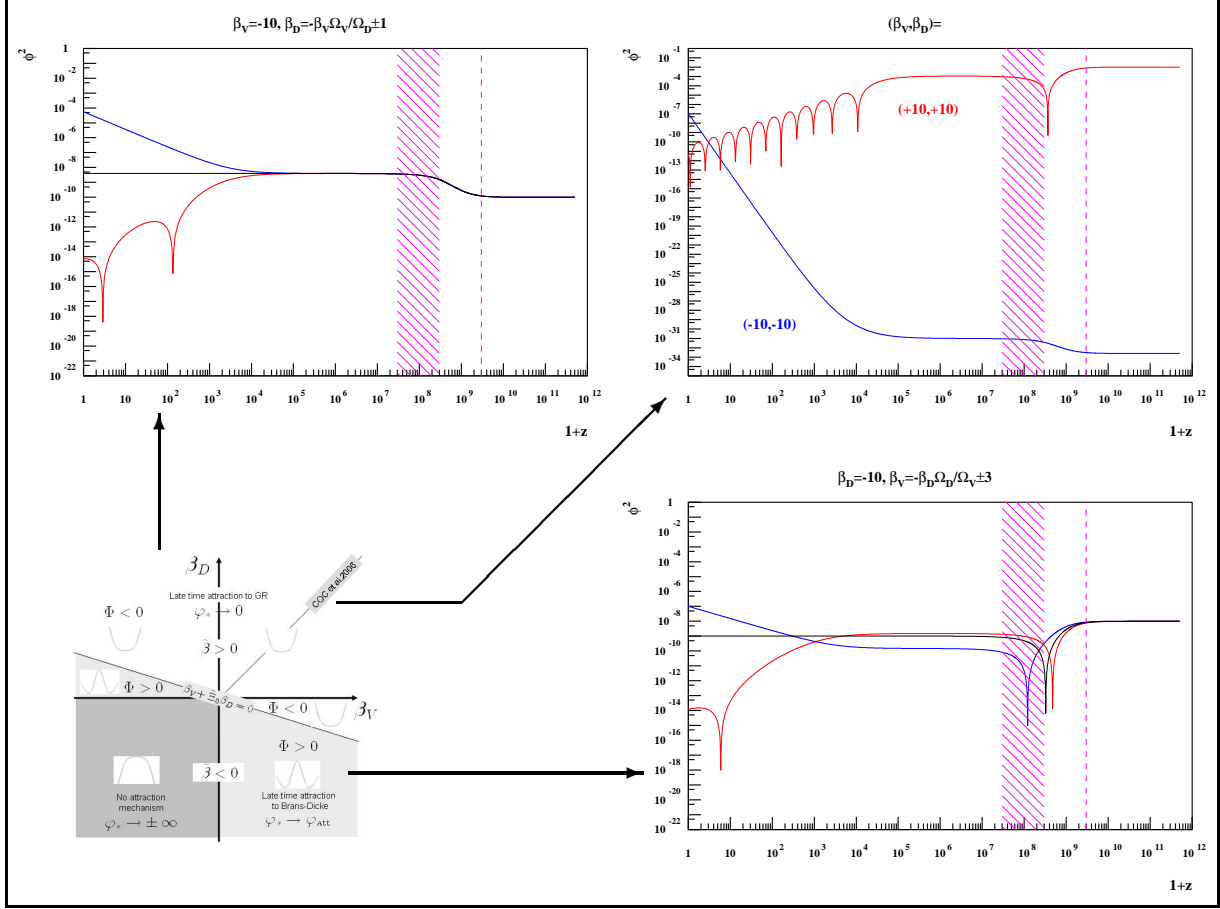


FIG. 7: (Lower left): Phase space of the solutions. (Upper-left) when  $\beta_V < 0$  the theory is dragged away from general relativity during BBN and then, depending on the sign of  $\tilde{\beta}$ , attracted towards or away from general relativity at late times. The field is at the minimum of the coupling function today only if  $\tilde{\beta} = 0$  (as seen by the horizontal line at late times). (Lower-right) when  $\beta_D < 0$  the theory is attracted toward general relativity during BBN and then, according to the sign of  $\tilde{\beta}$  attracted or not toward general relativity at late time. (Upper-right) Both  $\beta$ s are positive and the theory is always attracted toward general relativity. The opposite is true when both  $\beta$ s are negative.

when  $\tilde{\beta} = 0$ . When  $\tilde{\beta} = -1$ , the field continues to evolve away from  $\varphi_*^2 = 0$  when matter domination sets in. However, and as discussed in detail in Ref. [22], there are many other mass thresholds prior to electron-positron annihilation and a  $\beta_V < 0$  model would have to be fine-tuned to be attracted close enough to general relativity today. We shall thus restrict our analysis to  $\beta_V > 0$ .

Models with  $\beta_V > 0$  are attracted toward general relativity during electron-positron annihilation (see discussion below). Then, if  $\beta_D < 0$ , the theory is either attracted toward general relativity or a Brans-Dicke theory depending on the sign of  $\tilde{\beta}$ . As the analysis above also shows, in the latter case the theory is attracted toward a value of  $\varphi_*$  different from  $\varphi_* = 0$ . Examples of models with  $\beta_V > 0$ , but  $\beta_D < 0$  and  $\tilde{\beta} = -3, 0, +3$  are shown in the lower right plot of Fig. 7. Each case moves towards the origin (and undergoes one oscillation about the origin) prior to and during BBN. At late times, we see again that the model with

$\tilde{\beta} > 0$  continues to evolve towards the origin after matter domination, while model with  $\tilde{\beta} < 0$  evolves away from general relativity. As before the case with  $\tilde{\beta} = 0$  shows no further evolution.

Finally, in the upper right panel of Fig. 7, we show an example of a model with  $\beta_D = \beta_V = +10$ . The field moves through the origin once during electron-positron annihilation, and then later continues to oscillate about the origin. For completeness, we also show an example with  $\beta_D = \beta_V = -10$  in this panel which shows the run away behavior at late times.

In conclusion, we will concentrate our analysis on the case in which both  $\beta_V$  and  $\beta_D$  are positive (see upper-right plot of Fig. 7). This corresponds to models that are attracted toward general relativity without involving a tuning of the different parameters and the initial conditions for the value of  $\tilde{\beta}$  to be positive.

### 3. Different regimes

Deep in the radiation era, the cosmological constant the dark matter and baryonic matter components are negligible so that Eq. (4.7) simplifies to

$$\frac{2}{3 - \varphi'^2} \varphi_*'' + \frac{2}{3} \varphi_*' = 0. \quad (4.14)$$

As a consequence, the field is frozen at a constant value and the initial conditions can be chosen as

$$\varphi_{*\text{in}}' = 0, \quad \varphi_* = \varphi_{*\text{in}} = \text{constant}.$$

Still in the radiation era, when the universe cools below the mass of some species,  $\chi$ , this species becomes non-relativistic and induces a non-vanishing contribution to the r.h.s. of Eq. (4.7). The most important mass threshold for the BBN predictions is the last of these thresholds, the one associated with electron-positron annihilation. Previous mass thresholds are also important and drive the scalar-tensor theory toward general relativity (see § III.A.3 of Ref. [22]). We assume that the dark sector is not affected by any mass thresholds after muon annihilations. In that case, we can neglect the effect of the dark sector and we end up with the same result as in Ref. [22],

$$\frac{2}{3 - \varphi_*'^2} \varphi_*'' + \frac{2}{3} \varphi_*' + \Sigma_e(T) \beta_V \varphi_* = 0, \quad (4.15)$$

with

$$\Sigma_e(T) = \frac{15}{\pi^4} \frac{g_e}{g_*(T)} z_e^2 \int_{z_e}^{\infty} \frac{\sqrt{x^2 - z_e^2}}{e^x + 1} dx. \quad (4.16)$$

This implies that we are driven toward general relativity during the electron-positron annihilation only if  $\beta_V > 0$  (see right half of Fig. 7).

After electron-positron annihilation, the universe is still dominated by radiation and the scalar field freezes at a constant value,  $\varphi_{*\text{out}}$ . BBN can place a constraint on the value of  $a_{\text{out}} = a(\varphi_{*\text{out}})$ . Unfortunately, this constraint depends on  $a_{\text{in}}$  which is unknown. To compare these constraints to those obtained in the Solar system, we need to relate  $a_{\text{out}}$  to  $a_0$ . Thus, our code integrates the evolution equation up to the present, so that we obtain

$a_0$  directly. For the particular case of a vanishing potential or as long as the field is slow rolling,  $\varphi' \ll 3$ , Eq. (4.7) takes the slightly simplified form

$$\frac{2}{3}\varphi_*'' + (1-w)\varphi_*' = -\frac{\beta_V + \beta_D \Xi_0 e^{\frac{1}{2}(\beta_D - \beta_V)(\varphi_*^2 - \varphi_{*0}^2)}}{1 + \Xi_0 e^{\frac{1}{2}(\beta_D - \beta_V)(\varphi_*^2 - \varphi_{*0}^2)}}\varphi_*. \quad (4.17)$$

Contrary to the case of a universal coupling (§ III.5 of Ref. [22]) this equation cannot be integrated analytically in the matter-radiation era.

The field is attracted toward its minimum and at late times we can assume that  $\varphi_* \ll 1$ , in which case the equation of evolution reduces to

$$\frac{2}{3}\varphi_*'' + (1-w)\varphi_*' + \omega^2\varphi_* = 0, \quad \omega^2 \equiv \frac{\beta_V + \beta_D \tilde{\Xi}_0}{1 + \tilde{\Xi}_0}$$

It follows that the field evolves as

$$\varphi_*(p) = e^{-\frac{3}{4}p} \left[ A \cos\left(\frac{3}{4}rp\right) + B \sin\left(\frac{3}{4}rp\right) \right], \quad (4.18)$$

$$e^{-\frac{3}{4}p} \left[ A \cosh\left(\frac{3}{4}rp\right) + B \sinh\left(\frac{3}{4}rp\right) \right], \quad (4.19)$$

respectively if  $\omega^2 < \frac{8}{3}$  and  $\omega^2 > \frac{8}{3}$  with

$$r \equiv \sqrt{\left|1 - \frac{8}{3}\omega^2\right|}.$$

This allows us to compute the period of the last oscillations,

$$\Delta p = \frac{8}{3} \frac{\pi}{r(\beta_V, \beta_D, \tilde{\Xi}_0)}. \quad (4.20)$$

Unfortunately we can not compute the phase, which is required in order to match to the solution in the radiation era.

An example of such an evolution is depicted in the left panel of Fig. 8 with  $\beta_V = \beta_D = +10$  as in the upper right of Fig. 7. Here we see the same oscillations scaled by  $e^{3p/2}$  as expected from Eq. (4.19) with period given by Eq. (4.20). In the right panel of Fig. 8, we show several cases (as labelled) showing the late time scaling and oscillations. We can see that the field remains frozen during the radiation era up to the kick during electron-positron annihilation. When the universe starts to be matter dominated the field undergoes damped oscillations with a period given by Eq. (4.20).

## B. Constraints

### 1. BBN

We proceed as in Ref. [22] and vary the baryon to photon ratio,  $\eta$ , the values of  $\beta_V$  and  $\beta_D$  as well as the initial conditions  $a_{\text{in}}$  but we assume that the other cosmological parameters are fixed to their standard values. We compute the light element abundances as a function

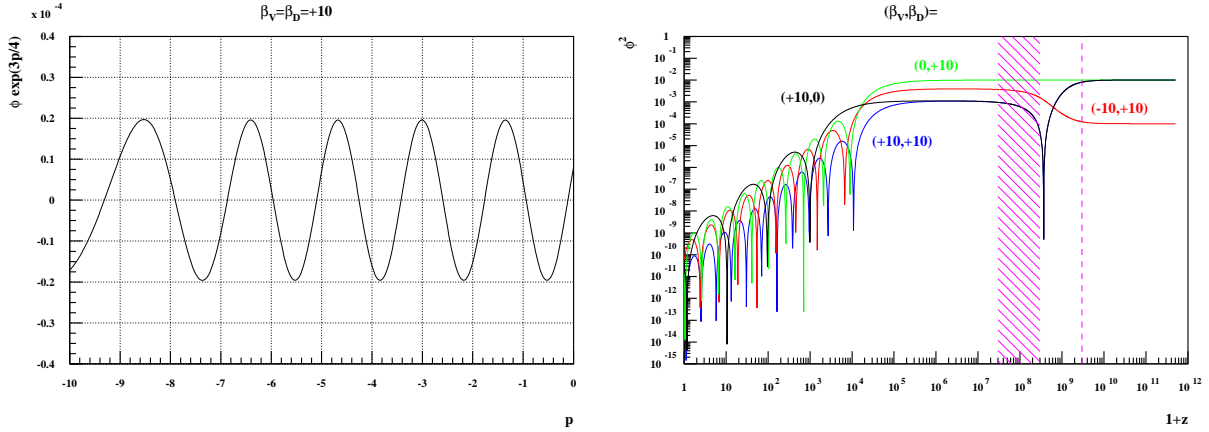


FIG. 8: (Left): Evolution of  $\varphi_* \exp(\frac{3}{4}p)$  as a function of redshift. The frequency of the oscillations depends on  $\beta_V$ ,  $\beta_D$  and the energy densities as in Eq. (4.20). (Right): Some solutions with  $\tilde{\beta} > 0$  summarizing the effect of  $\beta_V$  during BBN and the evolution during the matter era.

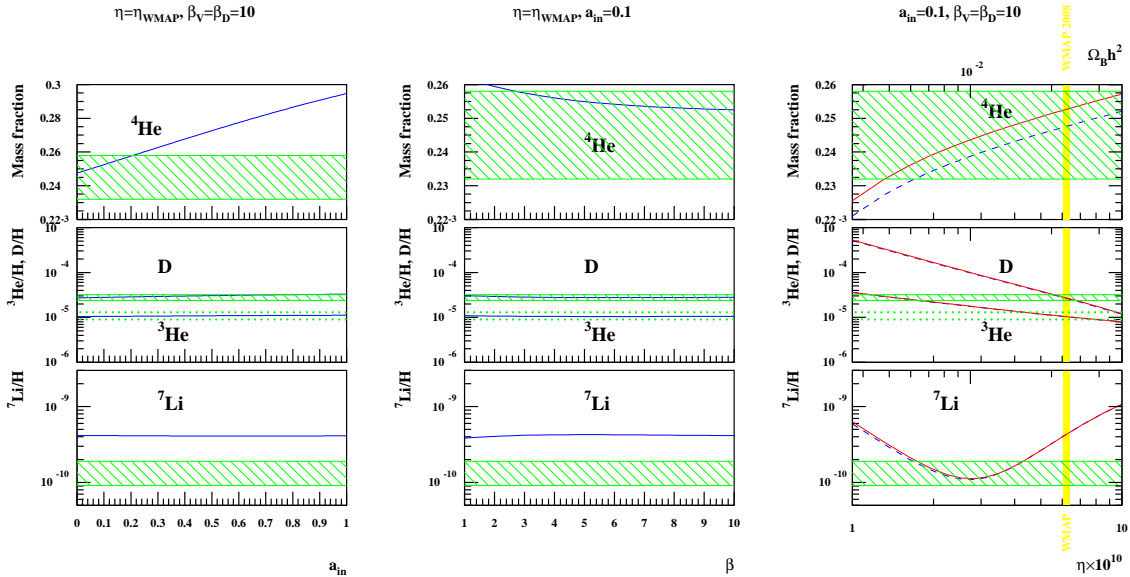


FIG. 9: (Left): Light element abundance as a function of  $a_{\text{in}}$  when  $\eta = \eta_{\text{WMAP}}$  and  $\beta_V = 10$ . (Middle): Same as a function of  $\beta_V$  when  $\eta = \eta_{\text{WMAP}}$  and  $a_{\text{in}} = 0.1$ . (Right): Same as a function of  $\eta$  for  $\beta_V = 10$  and  $a_{\text{in}} = 0.1$ . The standard model is shown by the lower (blue) dashed curves.

of these four parameters. Fig. 9 shows the effect of the independent variation of each of these parameters. This allows one to set the BBN constraints on these parameters which are then propagated until today to infer constraints on  $\alpha_{V0}$ ,  $\beta_V$  and  $\beta_D$ . Fig. 10 summarizes these constraints on the  $(\beta_V, \beta_D)$  plane obtained from BBN.

In the left panel of Fig. 9, we show the resulting light element abundances as a function of the parameter  $a_{\text{in}}$  for fixed values of  $\beta_V = \beta_D = 10$  and  $\eta$  fixed at the WMAP value of  $6.23 \times 10^{-10}$  [4]. As one can see in this panel and others to the right, there is very little

dependence of  ${}^3\text{He}$ , D, or  ${}^7\text{Li}$  on either  $a_{\text{in}}$  or  $\beta_V$ . Note that the  ${}^7\text{Li}$  abundance is always in excess of the observations for this value of  $\eta$  (see e.g. Ref. [48]). In contrast, there is a relatively strong dependence of the  ${}^4\text{He}$  abundance with  $a_{\text{in}}$ . The shaded regions correspond to the range of the observational determinations as described in Appendix C. The upper limit on the  ${}^4\text{He}$  abundance of 0.259 places a constraint on  $a_{\text{in}} \leq 0.2$ , when  $\beta_V = 10$ . In the middle panel of Fig. 9, we show the element abundances as a function of  $\beta_V$  for fixed  $a_{\text{in}} = 0.1$  and the WMAP value for  $\eta$ . At this value of  $a_{\text{in}}$ , we find a lower bound on  $\beta_V > 2.8$ . Finally, in the right panel of Fig. 9, we show the abundances as a function of  $\eta$  for fixed  $a_{\text{in}} = 0.1$  and  $\beta_V = \beta_D = 10$ . This choice of parameters leads to an increase in the  ${}^4\text{He}$  abundance of roughly 0.005 over the standard model with  $a_{\text{in}} = 0$  and  $\beta_V = 0$  as shown by the lower set of blue dashed curves.

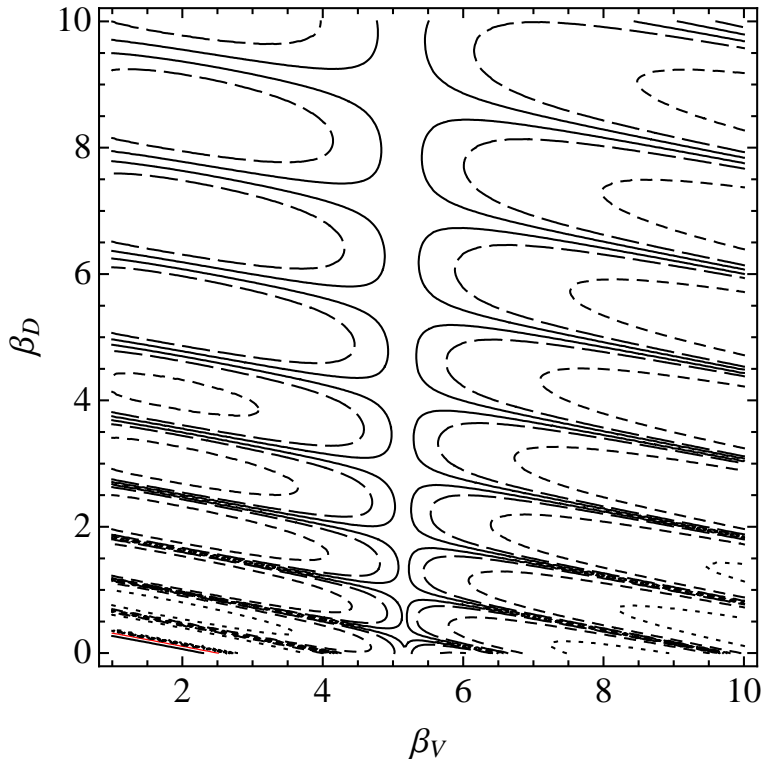


FIG. 10: Constraints on  $\alpha_{V0}$  in the plane  $(\beta_V, \beta_D)$ , respectively for  $\log \alpha_{V0} = -5$  (solid line),  $-4.5$  (long dashed lines)  $-4$  (dashed lines) and  $-3.5$  (dotted lines). The red line in the lower left corner shows the solar system constraint of  $\log \alpha_{V0} = -2.5$

Now, for each value of the pair  $(\beta_V, \beta_D)$ , we can compute the abundances of  ${}^4\text{He}$ ,  ${}^3\text{He}$ , D and  ${}^7\text{Li}$  as a function of  $a_{\text{in}}$  which allows us to constrain the values of this parameter from the observational data. We have set  $\eta = \eta_{\text{WMAP}}$ , though in principle, one could derive combined constraints on the pair of inputs  $(a_{\text{in}}, \eta)$ . One can check that this is a safe approximation and that the deviations from general relativity for the models considered do not lead to significant CMB deviations [23]. Then, this constraint on  $a_{\text{in}}$  can be propagated to get a constraint on the value of  $\varphi_*$  today, or equivalently on  $\alpha_{V0}$ .

The result of this analysis is depicted in Figure 10. This figure can be understood as follows. First we see that almost everywhere on the plane the solar system bound,  $\alpha_{V0}^2 < 10^{-5}$ , is satisfied (the area above the red line barely visible in the lower left corner);

see Eq. (B2). Second, for a given value of  $(\beta_V, \beta_D)$  we can read off the maximum value of deviation from general relativity that can be achieved in the Solar system once BBN constraints are satisfied. The result from Ref. [22] corresponds to the cut  $\beta_V = \beta_D$  of Fig. 10. Figure 10 shows clear structure with two sets of minima: (1) a set of parallel lines with increasing periodicity and (2) a vertical line close to  $\beta_V \sim 5$ . Let us now try to understand this behavior.

First, the periodicity seen in this figure is not directly related to the period (4.20) of the time evolution of  $\varphi_*$  but rather on the phase of this solution when evaluated at  $p = 0$ . Since we do not have an analytical solution in radiation-matter era, as in Ref. [22], our discussion can only be approximate but will still shed some light on our result. During the radiation era, but after BBN, the field is frozen at a value  $\varphi_{\text{out}*}$ . Assuming that at the time of matter-radiation equality,  $p_{\text{eq}}$ ,  $\varphi_{\text{eq}*} \simeq \varphi_{\text{out}*}$ , we can obtain a solution for  $\varphi_*$  at late times by matching the solution (4.18) to the constant solution at  $p_{\text{eq}}$  so that

$$\varphi_* = \varphi_{\text{out}*} e^{-\frac{3}{4}(p-p_{\text{eq}})} \cos \left[ \frac{3}{4} r (p - p_{\text{eq}}) \right]. \quad (4.21)$$

It follows, then, that the value of the scalar field today is given by

$$\varphi_{0*} = \varphi_{\text{out}*} e^{\frac{3}{4} p_{\text{eq}}} \cos \left[ \frac{3}{4} r p_{\text{eq}} \right], \quad (4.22)$$

which illustrates that the oscillations of  $\varphi_{0*}$ , and thus of  $\alpha_{V_0}$ , as a function of the two parameters  $(\beta_V, \beta_D)$ , are due to the oscillations of  $\varphi_{*0}$  as a function of  $r$  and are thus determined by the phase at the time of matching. To determine the points at which  $\varphi_{*0} = 0$ , we need the value of  $p_{\text{eq}}$  that is determined by imposing that  $\rho_{\text{mat}} + \rho_D = \rho_{\text{rad}}$ . This leads to

$$e^{-p_{\text{eq}}} = \Xi_0 \frac{\bar{A}(\varphi_{\text{eq}*})}{A_V(\varphi_{0*})}. \quad (4.23)$$

The almost horizontal periodic structure in Fig. 10 is related to the solution such that  $\varphi_{0*} = 0$ . When this happens,  $\tilde{\Xi}_0 = \Xi_0$  and  $A_V(\varphi_{0*}) = 0$  and these zeros occur when  $\frac{3}{4} r p_{\text{eq}} = n\pi$  with  $n \in \mathbb{N}$ , that is when

$$\sqrt{\frac{8}{3} \frac{\beta_V + \beta_D \Xi_0}{1 + \Xi_0}} - 1 = \frac{4}{3} n \frac{\pi}{\ln \frac{\Omega_{\text{mat}0}}{\Omega_{\text{rad}0}} + \frac{1}{2} a_{V\text{out}} + \ln \left( 1 + \Xi_0 e^{\frac{\beta_D - \beta_V}{\beta_V} a_{V\text{out}}} \right)}.$$

Now, since the dark sector does not influence the dynamics during electron-positron annihilation,  $\varphi_{\text{out}*}$  depends only on the values of  $\varphi_{\text{in}*}$  and  $\beta_V$ . This complicated relation is depicted in Fig. 2 of Ref. [22]. From this analysis, we argued that  $a_{V\text{out}}$  is at most of order  $10^{-1}$ - $10^{-2}$ . This implies that we expect the denominator of the r.h.s. of the previous expression to be dominated by  $\ln \frac{\Omega_{\text{mat}0}}{\Omega_{\text{rad}0}}$ . Thus, the positions in the plane  $\beta_V, \beta_D$  for which  $\alpha_{V_0} = 0$  (and as a consequence  $\alpha_{D_0} = 0$ ) corresponds to a set of parallel lines  $\mathcal{C}_n$  determined by

$$\beta_V + \beta_D \Xi_0 = \frac{3}{8} (1 + \Xi_0) \left[ \left( \frac{4n\pi}{3 \ln \frac{\Omega_{\text{mat}0}}{\Omega_{\text{rad}0}}} \right)^2 + 1 \right]. \quad (4.24)$$

This explains why the spacing between  $\mathcal{C}_n$  and  $\mathcal{C}_{n+1}$  grows almost linearly and is mainly determined by  $\Xi_0$  and  $\Omega_{\text{mat}0}/\Omega_{\text{rad}0}$ , which arises from the fact that the oscillations are related

by the time of matching. The slope is determined by  $\Xi_0$  since it characterizes the evolution during the matter era.

Let us now turn to the second feature in Fig. 10, that is, the vertical line on which  $\alpha_{V0} = 0$ . The relation between  $\varphi_{\text{out}}$  and  $\varphi_{\text{in}}$  is not monotonous and is determined mainly by  $\beta_V$  (see Figure 2 of Ref. [22] that shows that it is periodic in  $\beta_V$  with a first minimum for  $\beta_V \sim 5$ ). Figure 11 shows how that the relation between  $\varphi_{\text{out}}$  and  $\varphi_{\text{in}}$  has indeed a minimum at  $\beta_V \sim 5$ . This implies that for these models  $\varphi_*$  freezes to a very small value after the electron-positron annihilation so that these models are more efficiently attracted toward general relativity.

In summary, we can obtain a good understanding of our numerical results and of the origin of the structures of the minima in Fig. 10. In particular, we found that the two sets of structures do not have the same physical origin, one is related to electron-positron annihilation and the second to oscillations in the matter dominated era.

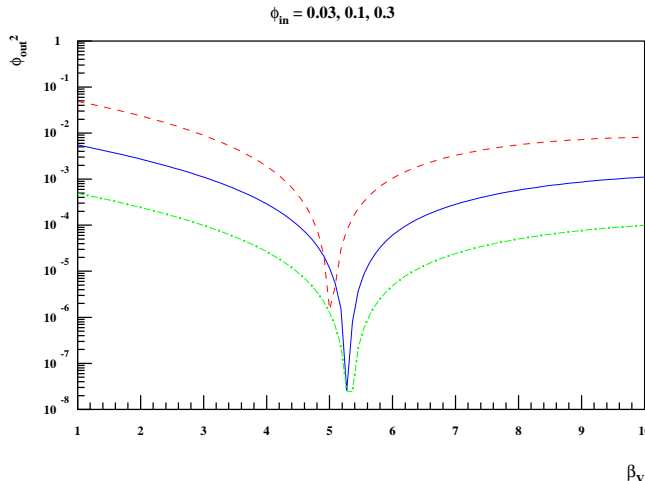


FIG. 11: Evolution of  $\varphi_{\text{out}*}$  as a function of  $\beta_V$  assuming that  $\phi_{\text{in}} = 0.03, 0.1$  and  $0.3$ . We see that the first minimum is obtained for  $\beta_V \sim 5$ , which corresponds to the vertical minimum of Fig. 10. There is a slight dependence of the minimum with respect to  $\phi_{\text{in}}$  and hence with the constraints provided by BBN.

## 2. Time variation of the gravitational constant

From Eq. (B3), using Eq. (2.19), the time variation of the gravitational constant is given by

$$\sigma = 2\alpha_V \left( 1 + \frac{\beta_V}{1 + \alpha_V^2} \right) \frac{\varphi'_*}{1 + \alpha_V \varphi'_*}, \quad (4.25)$$

where  $\sigma \equiv H^{-1} d \ln G_{\text{cav}} / dt$  is constrained by Eq. (B5), i.e. we must have  $|\sigma_0| < \Sigma_0$ , where  $\Sigma_0$  is the experimental upper bound on  $\sigma$  today; see Eq. (B5).

Assuming we are in slow-roll today, we deduce that

$$(1 + \Omega_{\Lambda 0}) \varphi'_{*0} \sim - \frac{\beta_V + \beta_D \Xi_0}{1 + X_0} \varphi_0.$$

We also deduce that the time variation of the gravitational constant today is

$$\sigma_0[\beta_V, \beta_D, \Xi_0, \alpha_{V0}] = 2\alpha_{V0} \frac{\left(1 + \frac{\beta_V}{1 + \alpha_{V0}^2}\right) (\beta_V + \beta_D \Xi_0)}{(1 + \Xi_0)(1 + \Omega_{\Lambda 0}) - \alpha_{V0}^2 (\beta_V + \beta_D \Xi_0)}. \quad (4.26)$$

Figure 12 shows the region of the parameter space  $(\beta_V, \beta_D)$  for which  $|\sigma_0| < \Sigma_0$  given the deviation from general relativity today, i.e.  $\alpha_{V0}$ . The contour plots can be understood as follows. Since  $\alpha_{V0}^2 \lesssim 10^{-5}$ , the second term in the denominator of Eq. (4.26) is negligible. Unless we have  $\beta$ s of order  $10^5$ , we conclude that

$$\frac{\sigma_0}{\Sigma_0 h} \sim 1.6 \times 10^{-2} \alpha_{V0} (1 + \beta_V) (\beta_V + \beta_D \Xi_0).$$

This shows that even if the dynamics of the field is influenced by  $\beta_D$  which can be very large, the Solar system constraints on  $\alpha_{V0}$  are so strong that it requires very high  $\beta_D$  to obtain a sizable time variation of the gravitational constant.

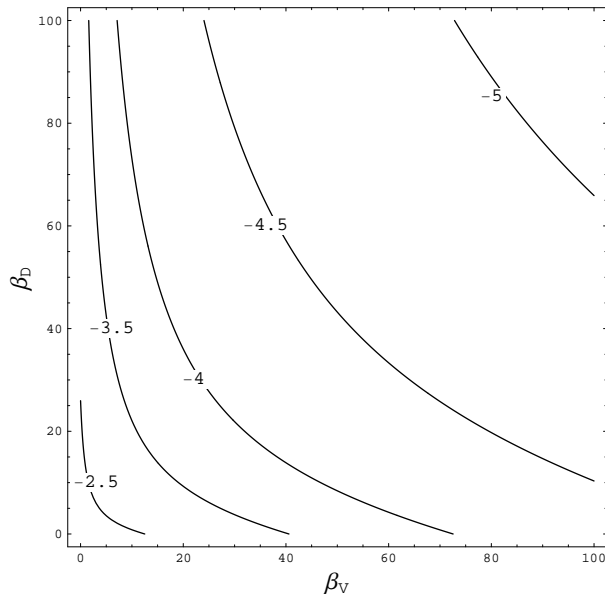


FIG. 12: Contour plot of the time variation of the gravitational constant in the plane  $(\beta_V, \beta_D)$  for different values of  $\log \alpha_{V0}$  indicated on each curve. The model has to lie on the lower-left part of the plot so that  $|\sigma_0| < \Sigma_0$ .

## V. CONCLUSIONS

For a theory of gravity universally coupled to matter, a scalar-tensor theory can be defined by a single coupling function  $A(\varphi)$  and a scalar potential. Such a theory can affect the evolutionary history of the universe, particularly in models of extended quintessence. Here we examined two types of quintessence models and examined the effects of the non-minimal coupling on the evolution of the quintessence field. For inverse power law quintessence models, we showed that the evolution towards a tracking solution is accelerated due to mass

thresholds in the radiation dominated epoch, and during the subsequent matter dominated epoch. In contrast, we saw that for quintessence models with defined minimum which is also a minimum of the coupling function, the non-minimal coupling to gravity has very little effect except at late times.

It is, however, possible that the dark sector of the theory couples to gravity differently from that of the visible sector. In this case, there is an additional coupling function as defined in Eq. (2.1). In this article, we have worked out the cosmological evolution of a scalar-tensor theory with distinct coupling functions for the coupling of the visible and dark sectors of the theory to gravity. We developed the qualitative features of the evolution with respect to the parameter space defined by  $\beta_V$  and  $\beta_D$  which are derived directly from the two coupling functions. We delineated those regions of the parameter space which are attracted towards general relativity, towards Brans-Dicke gravity, or towards a runaway solution. For those theories with a late time attraction to general relativity, we also derived additional constraints on the parameter space from BBN and precision gravitational tests. In particular, it was shown that in this class of models constraints more stringent than those derived from the Solar system can be obtained from BBN. This provides some insight on the equivalence principle between the visible and dark sectors.

### Acknowledgements

The time consuming part of the computations was performed on the computational grid GRIF (Grille de production pour la Recherche en Ile de France, <http://grif.fr>) and we thank Christophe Diarra for his help during the implementation of the code. We thank Carlo Schimd for his help in producing Fig. 10 and Gilles Esposito-Farèse and Cyril Pitrou for discussions. The work of KAO was partially supported by DOE grant DE-FG02-94ER-40823.

### APPENDIX A: NUMERICAL IMPLEMENTATION

From a numerical point of view, it is easier to integrate the Einstein equations in the Einstein frame while using the cosmic time  $t$  in the MJF. The expressions for the energy densities of the visible sector are trivial in the MJF, where they can be integrated analytically. It follows that the system reduces to

$$\frac{d\varphi_*}{dt} = A_V^{-1} \psi_* \quad (\text{A1})$$

$$\frac{d\psi_*}{dt} = -A_V^{-1} \left[ 3H_* \psi_* + \frac{dV}{d\varphi_*} + 4\pi G_* A_V^4 (\alpha_D \rho_D + \alpha_{\text{mat}} \rho_{\text{mat}}) \right] \quad (\text{A2})$$

$$H_*^2 = \frac{8\pi G_*}{3} A_V^4 (\rho_D + \rho_{\text{mat}} + \rho_{\text{rad}}) + \frac{1}{3} \psi_*^2 + \frac{2}{3} V - \frac{K}{R_*^2} \quad (\text{A3})$$

$$\frac{d\rho_{\text{rad}}}{dt} + 4H \rho_{\text{rad}} = 0, \quad (\text{A4})$$

$$\frac{d\rho_{\text{mat}}}{dt} + 3H \rho_{\text{mat}} = 0, \quad (\text{A5})$$

$$\frac{d\rho_D}{dt} + 3H \rho_D = A_V^{-1} (\alpha_D - \alpha_V) \rho_D \psi_*, \quad (\text{A6})$$

$$H = A_V^{-1} [H_* + \alpha_V \psi_*]. \quad (\text{A7})$$

Note the asymmetry in the coupling functions,  $A$ , arises from the fact that we have inserted the MJF energy densities rather than those defined in the EF. The last equation is necessary to derive the Hubble parameter in the MJF where the nuclear reactions are integrated.

## APPENDIX B: LOCAL CONSTRAINTS

The deviation from general relativity are constrained in the Solar system. These deviations are usually summarized by constraints on the post-Newtonian (PPN) formalism [49]. It is a general formalism that introduces 10 phenomenological parameters to describe any possible deviation from general relativity at the first post-Newtonian order [49]. The formalism assumes that gravity is described by a metric and that it does not involve any characteristic scale. In our particular case, it is necessary that the scalar field is light so that a Yukawa interaction on the scale of the solar system is not induced.

Since all of the matter in our Solar system stems from the visible sector (i.e. the dark matter component of the Sun and planets is supposed to be negligible), the two Eddington parameters (see Refs. [49, 50]) can be expressed in terms of the values of  $\alpha_V$  and  $\beta_V$  today as

$$\gamma^{\text{PPN}} - 1 = -\frac{2\alpha_{V0}^2}{1 + \alpha_{V0}^2}, \quad \beta^{\text{PPN}} - 1 = \frac{1}{2} \frac{\beta_{V0} \alpha_0^2}{(1 + \alpha_{V0}^2)^2}. \quad (\text{B1})$$

Solar System experiments set strong limits on these parameters. The perihelion shift of Mercury implies [51]  $|2\gamma^{\text{PPN}} - \beta^{\text{PPN}} - 1| < 3 \times 10^{-3}$ , the Lunar Laser Ranging experiment [52] sets  $4\gamma^{\text{PPN}} - \beta^{\text{PPN}} - 3 = -(0.7 \pm 1) \times 10^{-3}$ . Two experiments give a bound on  $\gamma^{\text{PPN}}$  alone, the Very Long Baseline Interferometer [53] sets  $|\gamma^{\text{PPN}} - 1| < 4 \times 10^{-4}$  and the measurement of the time delay variation to the Cassini spacecraft near Solar conjunction [54]  $\gamma^{\text{PPN}} - 1 = (2.1 \pm 2.3) \times 10^{-5}$ .

These two last bounds imply that  $\alpha_{V0}$  has to be very small, typically

$$\alpha_{V0}^2 < 10^{-5} \quad (\text{B2})$$

while  $\beta_{V0}$  can still be large [55]. Binary pulsar observations imply  $\beta_{V0} \gtrsim -4.5$ . Note that even though  $\beta_0$  is not bounded above by experiment, we will assume that it is not very large,

typically we assume  $\beta_{V0} \lesssim 100$ , so that the post-Newtonian approximation scheme makes sense. Note that none of these observations constrain the dark sector and  $(\alpha_{D0}, \beta_{D0})$  are completely free.

Since Cavendish experiment and planets are composed only of baryonic matter, we deduce that the gravitational constant is given by

$$G_{\text{cav}} = G_* A_V^2 (1 + \alpha_V^2). \quad (\text{B3})$$

Using  $p$  as the time variable as defined in Eq. (2.20), the time variation of the gravitational constant today determines the time derivative of  $\varphi_*$  today

$$2\alpha_{V0} \left[ 1 + \frac{\beta_{V0}}{1 + \alpha_{V0}^2} - \frac{\Sigma_0}{2} \right] \left. \frac{d\varphi_*}{dp} \right|_0 = \Sigma_0. \quad (\text{B4})$$

Experimentally, this is bounded [56] by

$$\frac{1}{G_{\text{cav}}} \frac{dG_{\text{cav}}}{dt} = \Sigma_0 H_0, \quad |\Sigma_0| < 5.86 \times 10^{-2} h^{-1}. \quad (\text{B5})$$

The new main feature compared to the models analyzed in Ref. [22] is that the dynamics of the scalar field depends on the dark sector coupling and thus on  $\alpha_D$ .

### APPENDIX C: BBN CONSTRAINTS

BBN is one of the most sensitive available probes of the very early Universe and of physics beyond the standard model. Its success rests on the concordance between the observational determinations of the light element abundances of D,  $^3\text{He}$ ,  $^4\text{He}$ , and  $^7\text{Li}$ , and their theoretically predicted abundances [57, 58]. Furthermore, measurements of the CMB anisotropies by WMAP [3, 4] have led to precision determinations of the baryon density or equivalently the baryon-to-photon ratio,  $\eta$ . The new WMAP 5-year data alone is  $\Omega_b h^2 = 0.02273 \pm 0.00062$  and is equivalent to  $\eta_{10, \text{CMB}} = 6.23 \pm 0.17$ , where  $\eta_{10} = 10^{10} \eta$ . Using the WMAP data to fix the baryon density, the light element abundances [59, 60, 61, 62, 63] can be quite accurately predicted. The wealth of the cosmological data are obtained from spectroscopic observations and compared directly with BBN predictions assuming the WMAP determination of  $\Omega_b h^2$ .

Note that the  $^4\text{He}$  abundance is often used as a sensitive probe of new physics (see e.g. [64]). This is due to the fact that nearly all available neutrons at the time of BBN end up in  $^4\text{He}$  and the neutron-to-proton ratio is very sensitive to the competition between the weak interaction rate and the expansion rate.

In the following, we briefly state the abundance measurements used in our analysis.

#### a. D/H

The best determinations of primordial D/H are based on high-resolution spectra in high-redshift, low-metallicity quasar absorption systems (QAS), via its isotope-shifted Lyman- $\alpha$  absorption. The seven most precise observations of deuterium in QAS give (see [65] and references therein) a weighted mean value of  $\text{D}/\text{H} = (2.82 \pm 0.21) \times 10^{-5}$  ( $1-\sigma$ ) in good agreement with BBN at the WMAP value of  $\eta$ . Note that the uncertainty quoted above is purely statistical and there remains considerable scatter in the data.

b.  ${}^4\text{He}$

${}^4\text{He}$  is observed in clouds of ionized hydrogen (HII regions), the most metal-poor of which are in dwarf galaxies. There is a large body of data on  ${}^4\text{He}$  in these systems [66, 67] for which an extended data set including 89 HII regions obtained  $Y_p = 0.2429 \pm 0.0009$  [67]. However, the recommended value is based on the much smaller subset of 7 HII regions, finding  $Y_p = 0.2421 \pm 0.0021$ .

${}^4\text{He}$  abundance determinations depend on several physical parameters associated with the HII region in addition to the overall intensity of the He emission line. These include, the temperature, electron density, optical depth and degree of underlying absorption. Unfortunately, there are severe degeneracies inherent in the determination of the  ${}^4\text{He}$  abundance [68]. Using a subset of the highest quality data from the sample of Izotov and Thuan [66], Monte Carlo methods were used to extrapolate the  ${}^4\text{He}$  abundance [69] which was determined to be  $Y_p = 0.2495 \pm 0.0092$ . Conservatively, it would be difficult at this time to exclude any value of  $Y_p$  inside the range  $0.232 - 0.258$ .

c.  ${}^7\text{Li}/H$

The systems best suited for Li observations are metal-poor halo stars in our Galaxy. Analyses of the abundances in these stars yields [70]  $\text{Li}/H|_p = (1.23_{-0.16}^{+0.34}) \times 10^{-10}$  when systematic uncertainties are included. The  ${}^7\text{Li}$  abundance based on the WMAP baryon density is predicted to be [60]  ${}^7\text{Li}/H = 4.15_{-0.45}^{+0.49} \times 10^{-10}$ . We note that a recent reanalysis of the  ${}^3\text{He}(\alpha, \gamma){}^7\text{Be}$  reaction, which is the most important  ${}^7\text{Li}$  production process in BBN, was considered in detail in [71]. When the new rate is used a higher  ${}^7\text{Li}$  abundance is found [48]  ${}^7\text{Li}/H = (5.24_{-0.62}^{+0.71}) \times 10^{-10}$ .

- 
- [1] A. G. Riess, *et al.* [Supernova Search Team Collaboration], *Astron. J.* **116** (1998) 1009; S. Perlmutter, *et al.* [Supernova Cosmology Project Collaboration], *Astrophys. J.* **517** (1999) 565.
  - [2] P. Astier, *et al.*, *Astron. Astrophys.* **447** (2006) 31.
  - [3] D. Spergel, *et al.*, *Astrophys. J. Suppl. Ser.* **170** (2007) 377.
  - [4] J. Dunkley, *et al.*, [arXiv:0803.0586].
  - [5] M. Kilbinger, *et al.*, [arXiv:0810.5129]; I. Tereno, *et al.*, [arXiv:0810.0055]
  - [6] J.-P. Uzan, in *Dark energy: theoretical and observational approaches*, Ed. P. Ruiz-Lapuente (Cambridge Univ. Press, 2009).
  - [7] J.-P. Uzan, *Gen. Relat. Grav.* **39** (2007) 307.
  - [8] J. Goodman, *Phys. Rev. D* **52** (1995) 1821.
  - [9] J.-P. Uzan, C. Clarkson, and G.F.R. Ellis, *Phys. Rev. Lett.* **100** (2008) 191303; J.-P. Uzan, F. Bernardeau, and Y. Mellier, *Phys. Rev. D* **77** (2008) 021301(R).
  - [10] R.R. Caldwell and A. Stebbins, *Phys. Rev. Lett.* **100** (2008) 191302.
  - [11] B. Ratra and P.J.E. Peebles, *Phys. Rev. D* **37**, (1988) 3406; C. Wetterich, *Nucl. Phys. B* **302** (1988) 668; R.R. Caldwell, R. Dave and P.J. Steinhardt, *Phys. Rev. Lett* **80** (1998) 1582; P.J.Steinhardt, L. Wang and I. Zlatev, *Phys. Rev. D* **59** (1999) 123504.

- [12] C. Schimd, *et al.*, *Astron. Astrophys.* **463** (2007) 405.
- [13] P. Jordan, *Nature (London)* **164** (1956) 637;  
M. Fierz, *Helv. Phys. Acta* **29** (1956) 128;  
C. Brans and R. Dicke, *Phys. Rev. D* **124** (1961) 925;  
P.G. Bergmann, *Int. J. Theor. Phys.* **1** (1968) 25;  
K. Nordtvedt, *Astrophys. J.* **161** (1970) 1059;  
R. Wagoner, *Phys. Rev. D* **1** (1970) 3209.
- [14] T. Damour and G. Esposito-Farèse, *Class. Quant. Grav.* **9**, 2093 (1992).
- [15] C.M. Will, *Living Rev. Rel.* **9** (2005) 3.
- [16] T. Damour and K. Nordtvedt, *Phys. Rev. Lett.* **70** (1993) 2217;  
*ibid.*, *Phys. Rev. D* **48** (1993) 3436.
- [17] J.-P. Uzan, *Phys. Rev. D* **59** (1999) 123510.
- [18] N. Bartolo, and M. Pietroni, *Phys. Rev. D* **61** (2001) 023518.
- [19] T. Damour, F. Piazza, and G. Veneziano, *Phys. Rev. Lett.* **89** (2002) 081601.
- [20] C. Wetterich, *JCAP* **0310** (2003) 002;  
M. Byrne and C. Kolda, [hep-ph/0402075];  
T. Chiba and K. Kohri, *Prog. Theor. Phys.* **107** (2002) 631;  
S. Lee, *Mod. Phys. Lett. A* **22** (2007) 2003.
- [21] T. Damour and B. Pichon, *Phys. Rev. D* **59** (1999)123502.
- [22] A. Coc, K.A. Olive, J.-P. Uzan, and E. Vangioni, *Phys. Rev. D.* **73** (2006) 083525.
- [23] A. Riazuelo, and J.-P. Uzan, *Phys. Rev. D* **65** (2002) 043525.
- [24] C. Schimd, J.-P. Uzan, and A. Riazuelo, *Phys. Rev. D* **71** (2005) 083512.
- [25] A. Riazuelo, and J.-P. Uzan, *Phys. Rev. D* **62** (2000) 083506.
- [26] J. Martin, C. Schimd, and J.-P. Uzan, *Phys. Rev. Lett.* **96** (2006) 061303.
- [27] K. A. Olive and M. Pospelov, *Phys. Rev. D* **65** (2002) 085044 ;  
D. Parkinson, B.A. Basset, and J.D. Barrow, *Phys. Lett. B* **578** (2004) 235.
- [28] J.-P. Uzan, *Rev. Mod. Phys.* **75** (2003) 403.
- [29] J.-P. Uzan, *AIP Conf. Proceedings* **736**(2004) 3; G.F.R. Ellis and J.-P. Uzan, *Am. J. Phys.* **73** (2005) 240.
- [30] C. Wetterich, *Phys. Lett. B* **655** (2007) 201 .
- [31] M. Kesden and M. Kamionkowski, *Phys. Rev. D* **74** (2006) 083007.
- [32] T. Damour, G.W. Gibbons, and C. Gundlach, *Phys. Rev. Lett.* **64**(1990) 123;  
T. Damour and C. Gundlach, *Phys. Rev. D* **43**(1991) 3873.
- [33] A. Füzfa and J.-M. Alimi, *Phys. Rev. D* **75** (2007) 123007;  
J.-M. Alimi and A. Füzfa, *JCAP* **0809** (2008) 014.
- [34] L. Amendola, *Phys. Rev. D* **62** (2000) 043511 .
- [35] G.R. Farrar, and P.J.E Peebles, *Astrophys. J.* **604** (2004) 1.
- [36] S. Das, P.-S. Corsaniti, and J. Khoury, *Phys. Rev. D* **73** (2006) 083509.
- [37] P. Brax, and J. Martin, *Phys. Rev. D* **75**, 083507 (2007).
- [38] A. Coc, *et al.*, *Phys. Rev. D* **76** (2007) 023511.
- [39] N. Kaloper and K. A. Olive, *Astropart. Phys.* **1**, 185 (1993); A. A. Tseytlin, *Int. J. Mod. Phys. D* **1**, 223 (1992).
- [40] S. Lee, K.A. Olive, and M. Pospelov, *Phys. Rev. D* **70** (2004) 083503.
- [41] C. Wetterich, *Phys. Lett. B* **561**, 10 (2003);  
L. Anchordoqui and H. Goldberg, *Phys. Rev. D* **68** (2003) 083513 ;  
E. J. Copeland, N. J. Nunes and M. Pospelov, *Phys. Rev. D* **69** (2004) 023501;

- D. S. Lee, W. Lee and K. W. Ng, *Int. J. Mod. Phys. D* **14** (2005) 335.
- [42] M. T. Murphy, J. K. Webb and V. V. Flambaum, *Mon. Not. Roy. Astron. Soc.* **345** (2003) 609;  
H. Chand, R. Srikanand, P. Petitjean and B. Aracil, *Astron. Astrophys.* **417** (2004) 853 .
- [43] A. I. Shlyakhter, *Nature* **264** (1976) 340;  
T. Damour and F. Dyson, *Nucl. Phys. B* **480** (1996) 37;  
Y. Fujii *et al.*, *Nucl. Phys. B* **573** (2000) 377.
- [44] K. A. Olive, *et al.*, *Phys. Rev. D* **66** (2002) 045022;  
K. A. Olive, *et al.*, *Phys. Rev. D* **69** (2004) 027701.
- [45] Y. Fujii and A. Iwamoto, *Phys. Rev. Lett.* **91** (2003) 261101.
- [46] P. Brax and J. Martin, *Phys. Lett. B* **468** (1999) 40.
- [47] V. Shani and L. Wang, *Phys. Rev. D* **62** (2000) 103517.
- [48] R. H. Cyburt, B. D. Fields and K. A. Olive, [arXiv:0808.2818 [astro-ph]].
- [49] C. Will *Theory and experiments in gravitational physics* (Cambridge University Press, Cambridge, England, 1993).
- [50] G. Esposito-Farèse and D. Polarski, *Phys. Rev. D* **63** (2001) 063504.
- [51] I.I. Shapiro, in *General Relativity and Gravitation 12*, N. Ashby *et al.* Eds. (Cambridge University Press, 1990), pp. 313.
- [52] J.G. Williams, X.X. Newhall, and J.O. Dickey, *Phys. Rev. D* **53** (1996) 6730.
- [53] S.S. Shapiro *et al.*, *Phys. Rev. Lett.* **92** (2004) 121101.
- [54] B. Bertotti, L. Iess, and P. Tortora, *Nature (London)* **425** (2003) 374.
- [55] T. Damour and G. Esposito-Farèse, *Phys. Rev. D* **54** (1996) 1474.
- [56] J.O. Dickey *et al.*, *Science* **265** (1994) 482.
- [57] R. H. Cyburt, B. D. Fields and K. A. Olive, *New Astron.* **6** (2001) 215.
- [58] A. Coc, *et al.*, *Phys. Rev. D* **65** (2002) 043510.
- [59] R. H. Cyburt, B. D. Fields and K. A. Olive, *Phys. Lett. B* **567** (2003) 227.
- [60] A. Coc, *et al.*, *Astrophys. J.* **600** (2004) 544.
- [61] R. H. Cyburt, *Phys. Rev. D* **70** (2004) 023505.
- [62] P. Descouvemont, *et al.*, *ADNDT* **88** (2004) 203.
- [63] A. Cuoco, *et al.*, *Int. J. Mod. Phys. A* **19** (2004) 4431.
- [64] R. H. Cyburt, B. D. Fields, K. A. Olive and E. Skillman, *Astropart. Phys.* **23** (2005) 313.
- [65] M. Pettini *et al.*, [arXiv:0805.0594 [astro-ph]]
- [66] Y. I. Izotov, T. X. Thuan, and V. A. Lipovetsky, *Astrophys. J.* **435**, 647 (1994) 647;  
*ibid.*, **108**, 1. (1997) 1;  
Y. I. Izotov and T. X. Thuan, *Astrophys. J.* **500** (1998) 188.
- [67] Y. I. Izotov and T. X. Thuan, *Astrophys. J.* **602** (2004) 200.
- [68] K.A. Olive, and E. Skillman, *New Astron.* **6** (2001) 119.
- [69] K. A. Olive and E. D. Skillman, *Astrophys. J.* **617** (2004) 29.
- [70] S.G. Ryan, *et al.*, *Astrophys. J. Lett.* **530** (2000) L57.
- [71] R. H. Cyburt and B. Davids, [arXiv:0809.3240 [nucl-ex]].